Multilayer Anisotropy Along the Alaska-Aleutians Subduction Zone

Andrew Birkey[1*] and Colton Lynner[1]

Department of Earth Sciences – University of Delaware[1]

*Corresponding author:

Department of Earth Sciences – University of Delaware

255 Academy St, Newark, DE 19716

Email: abirkey@udel.edu

Summary

Increasing evidence from seismic methods shows that anisotropy within subduction zones should consist of multiple layers. To test this, we calculate and model shear wave splitting across the Alaska-Aleutians Subduction Zone (AASZ), where previous studies have argued for separate layers of anisotropy in the subslab, slab, and mantle wedge. We present an updated teleseismic splitting catalog along the span of the AASZ, which has many broadband seismometers recently upgraded to three components. Splitting observations are sparse in the Western Aleutians, and fast directions are oriented generally trench parallel. There are significantly more splitting measurements further east along the AASZ. We identify six regions in the Central and Eastern Aleutians, Alaskan Peninsula, and Cook Inlet with a high density of splits suitable for multilayered anisotropy analyses. These regions were tested for multilayer anisotropy, and for five of the six regions we favor multiple layers over a single layer of anisotropy. We find that the optimal setup for our models is one with a dipping middle layer oriented parallel to paleospreading. A prominent feature of our modeling is that fast directions above and below the dipping layer are generally oriented parallel to the strike of the slab. Additionally, we lay out a framework for robust and statistically reliable multilayer shear wave splitting modeling.

Keywords: Seismic anisotropy; Dynamics of lithosphere and mantle; Mantle processes; Subduction zone processes

1. Introduction

Insights from a variety of seismic methods such as receiver functions (e.g., Wirth and Long, 2012), surface wave analyses (e.g., Liu et al., 2022), and shear wave splitting (e.g., Reiss et al., 2018) have shown that there are multiple layers of anisotropy in subduction zones. Analyzing bulk seismic anisotropy, which in the upper mantle generally arises from the macroscopic alignment of olivine crystals (e.g., Karato et al., 2008), is important in assessing ongoing mantle dynamics. The most common method to image anisotropy, teleseismic shear wave splitting (e.g. Long and Silver, 2009), is path-integrated. Any anisotropy existing from the core-mantle boundary to the receiver will be sampled by the seismic phases of interest (e.g., SKS, SKKS, PKS, collectively termed XKS). Untangling the contributions from multiple layers to total shear wave splitting requires forward modeling (e.g., Silver and Savage, 1994). An excellent location to test for and model these possible anisotropic layers is the Alaska-Aleutians Subduction Zone (AASZ, see **Fig. 1**). Previous teleseismic (e.g., Lynner, 2021; McPherson et al., 2020; Yang et al., 2021), local (e.g., Karlowska et al., 2020; Lynner et al., 2024; Richards et al., 2021), and source-side (Lynner and Long, 2014; Walpole et al., 2017) shear wave splitting studies, as well as surface-wave (Feng et al., 2020; Wang and Tape, 2014) and body-wave (Gou et al., 2019; Liu et al., 2022; You and Zhao 2012) tomography studies have suggested that seismic anisotropy varies vertically within the subduction zone.

We provide new teleseismic splitting measurements along the length of the AASZ, a roughly 3000-km region that has only recently been fully instrumented (with more deployments planned). Within the AASZ, slab age decreases from ~80 Myr in the west to ~45 Myr in the east (Heuret and Lallemand, 2005), with slab dip generally shallowing from west to east (Lallemand et al., 2005). The northeastern portion of the subduction zone likely has toroidal flow around the slab edge (e.g., Jadamec and Billen, 2012), which induces complex seismic anisotropy and mantle deformation (Yang et al., 2021).

Anisotropy in subduction zones exists in four likely regions: the subslab mantle, the slab, the suprabslab mantle wedge, and the upper plate. Subslab anisotropy may result from entrained flow associated with the slab (Faccenda and Capitanio, 2013; Walpole et al., 2017) or from more complicated asthenospheric flow (Long and Silver, 2009; Packzowksi et al., 2014). Both trench parallel and perpendicular subslab fast directions have been reported in the subslab mantle of the AASZ (e.g., Lynner and Long, 2014; Walpole et al., 2017). Debate exists regarding the strength of anisotropy in the subducting slab, though Long and Silver (2009) argue that it likely has a minimal contribution globally. Other studies, however, suggest slabs may have significant anisotropy due to fabrics arising from bending-induced faults coupled with dehydration reactions (Faccenda et al., 2008; Healy et al., 2009; Lee et al., 2020, 2021) or due to fossil anisotropy related to paleospreading (Audet 2013; Chen et al., 2015; Song and Kim, 2012).

Mantle wedge anisotropy may arise from two-dimensional corner flow (e.g., Hall et al., 2000; Long et al., 2007), olivine fabric transitions due to changes in temperature, pressure, and hydration (e.g., Jung, 2017; Jung and Karato, 2001; Jung et al., 2006), or changes in flow direction linked to the slab (e.g., Faccenda and Capitanio, 2012; Jadamec and Billen, 2010; Long and Silver, 2008). The upper plate likely contributes the least anisotropy in subduction zones, with most estimates placing an upper bound on crustal delay times of 0.3 seconds (Savage, 1999; Silver, 1996). Upper plate lithosphere may contribute if it is thicker and has fossil anisotropy, as in continents (e.g., Fouch and Rondenay, 2006; Silver, 1996). However, the dynamics of subduction zones likely thins the upper plate through increased heating (McKenzie, 1969), slab dehydration (Arcay et al., 2006), and mantle convection (Currie et al., 2008). In the AASZ we have good constraints on subslab anisotropy from source-side splitting (Lynner and Long, 2014; Walpole et al., 2017) and mantle wedge/upper plate anisotropy from local splitting (Karlowska et al., 2021; Lynner et al., 2024; Richards et al., 2021; Yang et al., 1995; Yang et al., 2021). Surface-wave and body-wave tomography studies provide information on anisotropy in the slab itself (Feng et al., 2020; Gou et al., 2019; Liu et al., 2022; You and Zhao, 2012; Wang and Tape, 2014).

The eastern portion of the AASZ has the needed density of shear wave splitting results to test for possible contributions to seismic anisotropy from different source layers: the subslab, slab, and mantle wedge. We perform forward modeling of multilayer anisotropy at six subregions within the AASZ and find that splitting in five subregions is statistically better fit by multiple layers of anisotropy. We find that our modeling favors flow in the subslab and mantle wedge oriented parallel or oblique to slab strike, consistent with previous studies (e.g., Liu et al., 2019; You and Zhao, 2012). Our modeling further demonstrates that a dipping middle layer with the a-axis of anisotropy oriented parallel to paleospreading is preferred.

1.1 Previous Teleseismic Splitting

Several recent studies have examined teleseismic shear wave splitting along portions of the AASZ, with most focused on the Alaskan subduction zone and eastern Aleutians (e.g., Christensen and Abers, 2010; Hanna and Long, 2012; Lynner, 2021; McPherson et al., 2020; Perttu et al., 2014; Richards et al., 2021; Venereau et al., 2019; Yang et al., 2021). There are very few published teleseismic shear wave splitting results for the western and central Aleutians (e.g., Long and Silver, 2008; McPherson et al., 2020) due to noisy conditions and a previous lack of instrumentation, though the global compilation of Long and Silver (2008) reports low delay times and trench-parallel fast directions.

The eastern Aleutians are better represented in published studies. Splitting delay times are generally low, and fast directions are mostly trench parallel (Hanna and Long, 2012; McPherson et al., 2020; Venereau et al., 2019). Trench parallel fast directions continue into the Alaskan peninsula (Lynner 2021; McPherson et al., 2020; Venereau et al., 2019). Outboard of the Alaskan peninsula, splitting becomes more variable. Lynner (2021) reported a transition from trench-parallel to trench-perpendicular fast directions near the Semidi segment and Shumagin gap, possibly linked to increased hydration and serpentinization.

Further northeast along the subduction zone, splitting is more complicated likely due to changes in the slab. In the Kenai Peninsula where the slab is relatively flat, fast directions are generally parallel to plate motion (McPherson et al., 2020; Richards et al., 2021). Events coming from the east, however, have splits that tend to be more trench parallel (McPherson et al., 2020; Perttu et al., 2014). The edge of the Pacific slab produces complex mantle flow, with splitting fast directions that curve around it (McPherson et al., 2020; Venereau et al., 2019). Splitting further inland in Central Alaska similarly seems linked to the dynamics of the slab (Christensen and Abers, 2010) and has been modeled with multiple layers of anisotropy (Yang et al., 2021).

1.2 Previous Local splitting

Splitting from local-S phases has a relatively small depth range over which it samples anisotropy compared to splitting from core-refracted XKS phases, and it provides excellent constraints on the mantle wedge (e.g., Long and Wirth, 2013). Local-splitting studies in the western and central Aleutians are generally lacking, though Long and Silver (2008) have fast directions oriented either trench parallel or trench oblique with up to 1.5 seconds of delay time. Lynner et al. (2024) report mostly trench parallel fast directions in the Central Aleutians, with delay times up to

3.0 seconds. In the Alaskan Peninsula, fast directions are mostly oriented trench parallel in the forearc, with a transition to trench perpendicular in the backarc; delay times vary from 0.1 to 3.0 seconds (Karlowska et al., 2020; Lynner et al., 2024; Richards et al., 2021; Yang et al., 1995). Local splitting in Central Alaska near the edge of the Pacific slab is oriented roughly trench oblique, with an average delay time of 0.4 seconds (Yang et al., 2021).

Previous studies demonstrated that there is disagreement between local and teleseismic splitting (Karlowska et al., 2020; Richards et al., 2021). It is important to note that a direct comparison is not possible given differences in frequency content and incidence angle of the rays. Regardless, both local and teleseismic studies have shown an increase in delay time with increasing mantle wedge path lengths (Christensen and Abers; Karlowska et al., 2020; Richards et al., 2021). This suggests that the mantle wedge is anisotropic, and that it is important to consider the contribution of anisotropy in the mantle wedge to the splitting of teleseismic XKS phases.

2. Methods

2.1 Shear wave splitting

We measured shear wave splitting at 152 broadband stations from 12 networks spanning the Western Aleutians through the Cook Inlet to the Kenai Peninsula of Alaska. Network details are in **Supplemental Text 1**. We measure splitting from the beginning of data availability for each station through August 2022. Splits were calculated using an updated version of the SplitLab package (Deng et al., 2017; Wüstefeld et al., 2008). We use an epicentral distance range of 90° to 160°, which includes optimal distances for PKS and SK(K)S phases. A lower magnitude cutoff of Mw 5.7 was used. Waveforms were band-pass filtered between 0.04 and 0.125 Hz.

The goal of shear wave splitting is to recover both the fast direction (phi) and delay time (dt) of the split wave. This provides information on the orientation of anisotropy through the fast direction, and the strength of anisotropy through the delay time. Reported splits were calculated using the minimum energy method (Silver and Chan, 1991). A common quality control for shear wave splitting is agreement between methods, so we also calculated solutions for the rotation correlation method (Bowman and Ando, 1987). Agreement within 15° between the two methods was required for a split to be considered good, and within 25° for fair. Additional quality controls on splitting included a signal-to-noise ratio above 5.0, a fast direction error of 25° or less, a delay time error of 0.7 seconds or less, and a correction from initially elliptical particle motion to rectilinear particle motion. Example splits are shown in **Supplemental Fig. S1**.

We only show fair and good splits in the figures here, though we included some poor splits with additional quality controls when modeling our results to improve backazimuthal distribution. Poor splits included in modeling were required to have error ranges of 35° or less for fast direction and 1.0 seconds for delay time. These splits also used the same values for the difference between methods. Finally, these poor splits were required to have the same elliptical-to-rectilinear particle motion as fair and good splits. Nulls (events with no evidence of splitting) were determined from their initial rectilinear particle motion and a disagreement in delay time between the minimum energy method (with high delay times) and the rotation correlation method (with low delay times, close to 0 seconds). An additional metric, splitting intensity (Chevrot, 2000), was calculated and used to determine nulls: this value is characteristically close to 0 for null events.

2.2 Multilayer Modeling

When a shear wave passes through multiple anisotropic layers, it undergoes splitting in each layer. The signal at the receiver is thus the aggregate of splitting in all layers and is commonly referred to as “apparent” splitting. For two layers of anisotropy, this results in backazimuthal periodicity of 90° for changes in fast directions and delay times (e.g., Silver and Savage, 1994). The inclusion of dipping layers or more than two layers of anisotropy yields more complicated backazimuthal variations, but still largely retains the 90° periodic nature of the two-layer case. This periodicity can be used to model the layers that generated the apparent splitting.

Layered anisotropy has been modeled from shear wave splitting in various regions and tectonic settings including subduction zones (e.g., Currie et al., 2004; Eakin and Long, 2013), transform plate boundaries (e.g., Özalbey and Savage, 1994; Silver and Savage, 1994), orogenic belts (e.g., Levin et al., 1999), rift zones (e.g., Gao et al., 2010; Hammond et al., 2014), cratonic regions (e.g., Nathan et al., 2021; Yang et al., 2014), and at ocean islands (e.g., Walker et al., 2001). Most layered anisotropic studies test for two layers, but some have tested for three layers when appropriate (e.g., Brechner et al., 1998; Eakin and Long, 2013; Levin et al., 1999; Yang et al., 2014). Silver and Savage (1994) laid out a method for modeling the effect of multiple layers of anisotropy, which we follow here.

We tested the possibility of one, two, and three layers of anisotropy. In the three-layered cases, we include models where the middle layer exhibits dipping axes of anisotropy to approximate the slab and models where all three layers are estimated to be horizontal. This gives us two suites of three-layered models: horizontal-dipping-horizontal (HDH) and horizontal-horizontal-horizontal (HHH). One- and two-layer models were calculated using M-Split, a MATLAB plugin (Abgarmi and Özacar, 2017). Three-layer models were generated following a similar algorithm using MSAT (Walker and Wookey, 2012), another MATLAB plugin which allows for layers with dipping axes of anisotropy. We will refer to the bottom layer in our models as the lower layer, and the topmost layer as the upper layer; the respective fast directions and delay times have the same terminology (see **Supplemental Fig. S2** for schematics of the model configurations). Note that because the modeling is carried out from a ray perspective, the lower layer is the first anisotropic layer the ray traverses. In addition to good and fair splits, we also included quality-controlled poor splits for our modeling. These had error ranges of 35° or less for fast direction and 1.0 seconds for delay time. We did not include nulls in our modeling.

For our layered anisotropy analyses, we implemented the unweighted misfit scheme of M-Split (Abgarmi and Özacar, 2017). The same misfit calculation was used for all our models. We also calculated bandfit misfit (Eakin and Long, 2013) for all models, which is an estimate of whether or not an observed apparent split matches the modeled split. For each measurement, if both the modeled fast direction and delay time were within the error bounds of the observed split, the bandfit misfit was set to zero. Otherwise, the bandfit misfit was set to one. This provides a helpful constraint on the number of measurements matched by each model.

Vertically propagating plane waves were assumed for all horizontal layers given the near-vertical incidence of teleseismic XKS phases. To generate anisotropy from a dipping layer, we assumed a hexagonal olivine symmetry that was approximated by a transversely isotropic mantle (Chevrot and van der Hilst, 2003) and rotated the Christoffel matrix using a change of basis (i.e., Bond, 1943; Walker and Wookey, 2012; see **Supplemental Text 2** for more information). This results in a dipping axis of symmetry for the anisotropy in the layer. The dipping layer is treated as having uniform thickness. For horizontal layers, we assumed that the fast direction and delay time were constant at all backazimuths. Thus all layers were approximated as horizontal.

The first step to model the dipping layers was determining appropriate slab parameters. The dipping layer is described by slab dip, anisotropic thickness, and the orientation of the a-axis of olivine (azimuth). Appropriate parameters were determined from Slab2 (Hayes et al., 2018). We defined a box around each region, and found values from Slab2 within this box (see **Supplemental Text 3** for the boundaries of each region). Because we modeled results at a regional scale, we tested a range of dips from Slab2. We tested various parameters to determine reasonable delay times, and ultimately chose a 30 km thick anisotropic layer to balance thickness and strength of anisotropy. This produced realistic delay times in the dipping layer (~0.5 seconds on average). There is a trade-off between the strength of anisotropy and the thickness of the dipping layer, so an identical effect could have been achieved using a thicker layer and weaker anisotropy. This choice in thickness is further motivated by previous studies that have argued anisotropy within the slab is likely limited to a relatively thin zone of less than 50 km (e.g., Audet, 2013; Faccenda et al., 2008). We also tested various orientations for the dipping layer, including strike of the slab, plate motion in a hotspot reference frame (Gripp and Gordon, 2002), and paleospreading determined from paleomagnetic data (Maus et al., 2009). Using a coarse grid (10° increments for fast direction, 0.2 second increments for delay time), we determined the best-fitting dip as the value with the lowest unweighted misfit (**Supplemental Table 1**).

With the appropriate dipping-layer parameters determined, we ran the models on a finer grid for two layers and all three dipping layer orientations (trench parallel anisotropy, plate motion anisotropy, paleospreading anisotropy). For two-layer and three-layer models with a dipping layer, fast directions were tested from -90° to 90° using a 3° increment. Delay times varied from 0.4 to 3.0 seconds with 0.1 second increments. We used a coarser grid for the HHH model: fast direction ran from -90° to 90° in 10° increments, with delay time running from 0.4 to 3.0 seconds in 0.2

second increments. For all setups, the model with the lowest unweighted misfit was deemed the best-fitting model. The final values used for all model configurations are shown in **Supplemental Table 1**. We also list the trench orientation as it is common for shear wave splitting studies in subduction zones to describe splits in relation to the trench (i.e., trench parallel or perpendicular). While slab strike and trench orientation are not necessarily linked, we note that for each modeled region the two are within 25° of one another, and therefore subparallel.

An important step in the layered modeling was to test against the null hypothesis of a single layer of anisotropy. We ran an F-test for nested models (Mendenhall and Sincich, 2016) to compare between one layer and multilayer models. This was necessary because there are differences in the degrees of freedom between each model type. We calculated the F-value as:

$$F = \frac{(m_1 - m_n)/m_n}{(df_1 - df_n)/df_n} \quad (1)$$

where m_1 and df_1 are the misfit and degrees of freedom for the one-layer model, and m_n and df_n are the misfit and degrees of freedom for the multi-layer model. We evaluated the F-value at a probability level of 0.05. Degrees of freedom were calculated by subtracting the number of parameters for each model from the number of data points being tested. For a single layer, there were two parameters (fast direction and delay time). For two-layer and HDH models, there were four (two fast directions, two delay times); for HDH, the strike of the dipping layer, thickness of the dipping layer, and dip of the dipping layer were set in the final modeling and therefore not being searched for. For the HHH models, there were six (three fast directions, three delay times).

M-Split performs a grid-search for the best-fitting fast direction and delay time for a single layer of anisotropy (i.e., there is no backazimuthal variation in either parameter). However, a direct comparison of misfit between models with different degrees of freedom is not possible. This is the utility of the nested model F-test, which considers the relative decrease in misfit compared to the decrease in degrees of freedom (more complex models have fewer degrees of freedom because more parameters are being searched for). Comparing the misfit of all models against the single-layer case using the F-test generally produces a suite of models that are statistically better than the single-layer case. This suite is a subset of the suite of models that is statistically indistinguishable from the lowest-misfit model for a given setup and degrees of freedom. For brevity, we will refer to this suite of models as robust multilayer models from here on out.

3. Results

3.1 Shear Wave Splitting Results

We made a total of 761 split and null shear wave splitting measurements at 152 stations. A total of apparent 309 splits were of either fair or good quality at 116 stations, and 155 nulls at 74 stations (**Fig. 2**). There are fewer apparent splits in the Western Aleutians than in the other regions. While station-averaged splitting parameters are often reported, we choose not to do so as our apparent splits exhibit significant backazimuthal variation that would be smoothed over with averaging. We begin by describing some general trends seen in our apparent splitting results.

Because one of the commonly reported orientations for fast directions in subduction zones is trench parallel, we compare apparent fast directions to the strike of the slab from Slab 2 (Hayes et al., 2018) according to longitude (**Fig. 3a**). The Western Aleutians have the fewest results, and apparent fast directions there are tightly clustered and close to slab strike. Moving further east, most apparent fast directions are not parallel to slab strike. We also compare apparent fast directions to longitude (**Fig. 3c**) and latitude (**Fig. 3d**). There is a general transition from negative fast directions in the west, to scattered fast directions in the east with a general bias toward more positive values. This is likely a reflection of the slab strike parallel nature of splits in the Western Aleutians. Apparent delay times vary across the entire region, with a minimum of 0.4 seconds and a maximum of 3.5 seconds (both on Akutan Island). We note that while this is large variation in apparent delay times, these two extrema also have different fast directions and come from different backazimuths, congruent with multiple layers of anisotropy. The only observed general trends in delay time are slightly lower values in the Western Aleutians, which range from 0.7 to 1.9 seconds (**Fig. 3e-f**). Low delay times are found throughout the region, but the range of values increases moving further to the east.

Apparent fast directions across most of the AASZ are scattered and vary backazimuthally. We identify six regions with a high density of splits that show potential systematic variations in fast directions (**Fig. 4**). Apparent splits in all these regions show complex splitting patterns, particularly for the Eastern Aleutians and Okmok. Such backazimuthal variation is diagnostic of either a dipping axis of anisotropy or multiple layers of anisotropy (Silver and Savage, 1994), with the former exhibiting 180° periodicity and the latter 90° periodicity. This observation, coupled with conclusions from previous studies in the AASZ, is a primary motivation for our modeling of multiple anisotropic layers.

3.2 Modeling Results

We chose to focus our modeling effort on six broader geographic subregions as this increased the backazimuthal coverage in splitting. Models are generated only for areas with more than 25 apparent splits (boxed regions in **Fig. 1a**). This includes, from west to east: Okmok (11 stations and 40 splits), the Eastern Aleutians (Akutan and Unalaska Islands, and Unimak; 17 stations and 66 splits), Katmai National Preserve (11 stations and 49 splits), Augustine Volcano (9 stations and 30 splits), Iliamna Volcano (6 stations and 33 splits), and Redoubt Volcano (6 stations and 38 splits). A list of the stations is provided in **Supplemental Text 4**. We were not able to adequately model any regions west of Okmok due to more limited data coverage.

Our statistical analyses show that for all configurations we are able retrieve robust multilayer models except for at Redoubt where multilayer models are not statistically distinguishable from a single layer. We therefore do not examine the single best-fitting model as is done in many studies since this may not be representative of the whole suite of robust models. Rather, we look for trends in the whole suite of robust multilayer models. An example is shown in **Fig. 5** for Okmok (where the dipping layer is oriented parallel to paleospreading), other fast direction histograms are shown in **Supplemental Figs. S3-6**. The fast directions appear to be better modeled than the delay times (e.g., Aragon et al., 2017; Yuan and Levin, 2014). This may be a result of the overestimation of delay times when using the minimum energy method (Monteiller and Chevrot, 2010). As with other modeling studies, we choose not to further consider delay times as part of our modeling (e.g., Aragon et al., 2017; Dubé et al., 2020; Nathan et al., 2021).

A comparison between model configurations for Okmok is shown in **Fig. 6**. The lower layer for all three setups seems to coalesce on a single value (between 15° and 40°). The upper layer in the two layer and HHH cases have similar values (~25° to 40°), but the HDH case yields a different result (clustered around -90°/90°). The middle layer for the HHH case is poorly constrained with only small peaks, a finding that is consistent across all regions. Histograms for all regions other than Redoubt are shown in **Supplemental Figs. S3-6** and the modal fast direction for each setup (i.e., the peak in the histogram) is shown in **Table 1**.

Other regions show similar trends as Okmok. In the Eastern Aleutians, lower layer fast directions for all three configurations are similar, clustering between 50° and 70°. There is slightly more spread in lower layer fast directions for the HHH case than for the two-layer and HDH cases. Upper layer fast directions for all three configurations are also similar with peaks between 25° and 40°, though the distributions have a large negative skew. For Iliamna, the main peak in lower layer fast directions for all three model configurations is between 50° and 70°. The two-layer and HDH cases have other smaller peaks that occur in roughly the same locations (near -40° and between 15° and 30°). The upper layers all have peaks between 30° and 50°, again with a negative skew. Histograms for all regions are addressed in further detail in **Section 4.2.**

4. Discussion

We find that the eastern portion of the AASZ has a sufficient number of shear wave splitting results to test for contributions from multiple layers of anisotropy. To analyze the nature of depth-dependent anisotropy in the AASZ, we tested our teleseismic splitting results against models with one, two, and three layers of anisotropy. An important consideration that is often ignored in layered modeling of shear wave splitting results is the possibility of a dipping layer. We include a dipping middle layer in our modeling with several tectonically derived fabrics (plate motion, slab strike, paleospreading). We identified six subregions with the need backazimuthal coverage to model the layered anisotropy signal (shown in **Fig. 1a**). Of these subregions, five have robust multilayer models. Below, we further discuss our preferred layered model in **Section 4.1**. We then compare the results of our modeling to tectonic constraints and previous splitting and tomography studies in **Section 4.2**. Finally, we lay out a method to produce robust layered models of shear wave splitting in **Section 4.3**.

4.1 Preferred Model

Apart from Redoubt, the best solution is one with three layers with a dipping middle layer of anisotropy. The lower layer likely represents the subslab mantle, the middle dipping layer likely represents the slab, and the mantle wedge is the upper layer. This is consistent with observations from other studies that have found at least three distinct regions of anisotropy within the AASZ. Source-side splitting studies suggest a subslab anisotropic signal (e.g., Lynner and Long, 2014; Walpole et al., 2017). Local-S splitting constraints show a significant mantle wedge component (Karlowska et al., 2020; Lynner et al., 2024; Richards et al., 2021; Yang et al., 1995; Yang et al., 2021), and teleseismic splitting studies (Richards et al., 2021) and anisotropic tomography (Gou et al., 2019; Liu et al., 2022; You and Zhao, 2012) show that the slab is anisotropic. We place less weight on the HHH models because they universally result in a middle layer that is poorly constrained by our splitting data (**Fig. 6**). Additionally, the HHH models generally provide broadly the same upper- and lower-layer solutions as the two-layer and HDH cases (**Supplemental Figs. S3-6**).

For all regions except Redoubt, there is a suite of models that are statistically better than the one-layer case. This demonstrates the necessity of testing the null hypothesis of a single layer of anisotropy. While two-layer solutions oftentimes have slightly lower misfits than three-layered cases, they are not statistically distinguishable given the difference in free parameters. Given the evidence from other seismic studies that the AASZ should have an anisotropic slab plus two additional layers of anisotropy, we prefer the HDH case to the two-layer one.

The final constraint that we place on our models is the orientation of the dipping layer. The choice of orientation for the dipping layer does not seem to have a large effect on the final solution (see the **Supplemental Figs. S8-9** for all the HDH histograms). We therefore must rely on tectonic and geologic information to infer the best orientation for the middle dipping layer. Global and regional surface wave tomography (Debayle and Ricard, 2013; Maggi et al., 2006), regional body wave tomography (Gou et al., 2019; You and Zhao, 2012), and body-wave travel times (Shearer and Orcutt, 1986) show evidence that the Pacific slab most likely has anisotropy oriented parallel to paleospreading. Studies of other slabs using receiver functions (Audet, 2013; Song and Kim, 2012) and shear wave splitting (Chen et al., 2015) have also provided evidence for paleospreading-parallel anisotropy in the subducting slab. We therefore prefer a model with the middle dipping layer oriented parallel to paleospreading, although we tested and report all three plausible middle layer cases here (**Supplemental Figs. S8-9**).

We will restrict our further discussion to the five regions (Augustine, the Eastern Aleutians, Iliamna, Katmai, and Okmok) that have HDH models statistically better than the single-layer case. The misfit for the multilayer cases at Redoubt is generally lower than for a single layer, but the difference in degrees of freedom results in statistically worse models. Future studies with increased backazimuthal coverage may resolve this, especially as two other regions near Redoubt (Augustine and Iliamna) are both fit well by multiple layers of anisotropy, and a previous study further to the northeast explicitly modeled multiple layers of anisotropy (Yang et al., 2021).

4.2 Tectonic Interpretation

In **Fig. 7**, we show histograms of our preferred model for the five regions with robust multilayer models. In general, both the upper- and lower-layer fast directions converge. The peak of each histogram is shown in **Table 1**. We begin by comparing the distribution of models to tectonic constraints, then previous splitting results. As noted in **Section 4.1**, our preferred model is one in which the lower layer of anisotropy is the subslab, the middle dipping layer (oriented parallel to paleospreading) is the slab, and the upper layer is the mantle wedge.

To test for possible tectonic contributions, we compare our robust multilayer model suites to plate motion in a hotspot reference frame (Gripp and Gordon, 2002), the strike of the slab (Hayes et al., 2018), and the paleospreading direction (Maus et al., 2009). These have all been suggested as possible orientations for anisotropy within subduction zones (e.g., Long and Wirth, 2013; Long and Silver, 2009). In this region, plate motion varies from 314° to 329° (Gripp and Gordon, 2002), or from -46° to -31° in the standard -90° to 90° shear wave splitting fast direction coordinate system. Except for secondary peaks for Iliamna at -27° and Katmai at -40°, plate motion does not correlate with modeled lower-layer fast directions. It also only correlates with secondary peaks in modeled upper-layer fast directions (for Katmai and the Eastern Aleutians at -40°). This suggests that slab-entrained asthenospheric flow or simple 2-D corner flow (which would both be oriented parallel to plate motion) is not a prominent feature of the modeled portions of the AASZ. Paleospreading estimated from paleomagnetic data in this region (Maus et al., 2009) is predicted to be roughly N-S (0°) or E-W (90°), and it appears to be an equally poor match for our modeled fast directions, only overlapping with the lower layer fast directions for Augustine near 90° and some of the upper layer fast directions for the Eastern Aleutians near 0°. This is not surprising, as paleospreading is most likely to cause anisotropy within the slab (as modeled here) rather than the subslab or mantle wedge.

A better correlation exists between the direction parallel to slab strike and our modeled fast directions. The lower layers for Katmai (33° fast direction, 40° slab strike – **Fig. 7e**), and the Eastern Aleutians (63° fast direction, 60° slab strike – **Fig. 7i**) have peaks at fast directions close to slab strike. While the misfit peak for Iliamna (63° fast direction) does not correspond to slab strike, a peak in the bandfit distribution does (20° fast direction, 25° slab strike – **Fig. 7a**). The peaks in upper-layer fast directions match slab strike at Augustine (33° fast direction, 35° slab strike – **Fig. 7d**) and Katmai (33° fast direction, 40° slab strike – **Fig. 7f**). Even in cases where the peak of the misfit distribution does not perfectly match slab strike, the two tend to be close in orientation. Because of this match, fast directions in both the upper and lower layers can be generalized as being either parallel or oblique to slab strike.

It is common in shear wave splitting studies in subduction zones to refer to fast directions relative to the orientation of the trench. Our modeling does not utilize trench orientation but rather slab strike. We show in **Supplemental Table 1** that for all modeled regions the two are within 25° of each other. This should allow us to compare our modeled results to previous studies that utilize terms such as "trench parallel" or "trench perpendicular" even though we do not expressly rely on trench orientation.

Previous teleseismic splitting studies in the region have generally not modeled multiple layers of anisotropy, except for Yang et al., (2021) who found that the edge of the Pacific Slab produced complex, likely toroidal flow. Splitting along the arc of the AASZ has mostly produced fast directions parallel to the trench (Christensen and Abers, 2010; Hanna and Long, 2012; Lynner, 2021; McPherson et al., 2020; Richards et al., 2021; Venereau et al., 2019), though local deviations exist. For instance, Lynner (2021) found a transition from trench-parallel to trench-perpendicular splits near the boundary between the Semidi segment and the Shumagin Gap. Teleseismic splitting studies have reported much more complexity in the northeast of the subduction zone near the edge of the slab (e.g., McPherson et al., 2020; Perttu et al., 2014; Richards et al., 2021). Where the mantle wedge is relatively thin, fast directions have largely been linked to subslab asthenospheric flow, both in cases where that flow is trench parallel (Lynner, 2021; McPherson et al., 2020) and where it is trench-perpendicular (Christensen and Abers, 2010; Hanna and Long, 2012; Perttu et al., 2014). Because teleseismic splitting has no depth constraints, we cannot directly compare previous results to our robust multilayer models. However, it is a useful confirmation of our own modeling that previous studies suggest anisotropy at various depths in the AASZ is roughly trench parallel.

We can rely on shear wave splitting from other phases for information on specific depths. We use the source-side splits of both Lynner and Long (2014) and Walpole et al. (2017) to constrain subslab anisotropy. Lynner and Long (2014) reported mostly trench-perpendicular source-side splits throughout the AASZ. However, they do find more complexity moving further east. Walpole et al. (2017) instead report mostly trench-parallel source-side splits, though they note this may be due to slight differences in methodology and data coverage. There are also different reference frames used for analysis, with Walpole et al. (2017) using a slab reference frame and Lynner and Long (2014) using a receiver-side anisotropy reference frame.

Mantle wedge anisotropy can be inferred through local-S splitting (e.g., Long and Wirth, 2013). Previous local-S splitting studies in the Alaskan Peninsula and Cook Inlet have reported trench-parallel fast directions in the forearc, and trench-perpendicular fast directions in the backarc (Karlowska et al., 2020; Richards et al., 2021). Augustine and Iliamna straddle the region between fore- and backarc, and both have a peak in upper-layer fast directions occurring close to slab strike (between 15° and 40° for Augustine, and between 30° and 45° for Iliamna – **Fig. 7b,d**). Katmai (on the Alaskan peninsula) also has an upper layer fast direction that matches slab strike (around 30°, **Fig. 7f**). Karlowska et al. (2020) report a mix of trench oblique and parallel splits here, which somewhat contradicts our own results. Lynner et al. (2024) also report fast directions in Katmai that are trench oblique (**Fig. 7f**). Further to the southwest, Yang et al. (1995) found roughly trench parallel fast directions at the Shumagin Gap. Where the mantle wedge is thicker, there is likely a contribution to teleseismic splitting as well (Christensen and Abers, 2010; Hanna and Long, 2012;

Richards et al., 2021; Yang et al., 2021). While teleseismic and local S-waves sample the same anisotropic structure, differences in frequency content and incidence angle make a direct comparison difficult. However, they still provide an essential constraint on anisotropy in the mantle wedge.

For the Eastern Aleutians, the source-side splitting from neither study (Lynner and Long, 2014; Walpole et al., 2017) matches the robust modeled lower-layer fast directions (**Fig. 7i**). Iliamna and Augustine do have some overlap with the source-side splitting results, but this overlap does not occur at the peaks (**Fig. 7a,c**). Both source-side splitting studies agree with a secondary peak in lower-layer fast directions for Katmai around -40° (**Fig. 7e**). The source-side splitting of Walpole et al. (2017) is close to the peak at Okmok (between 15° and 30° – **Fig. 7g**), whereas there is no overlap for the source-side splits of Lynner and Long (2014). Some caveats apply to our comparison between robust modeled lower-layer fast directions and source-side splitting. Events used to analyze the AASZ from Walople et al. (2017) come from a limited range of backazimuths and epicentral distances. Lynner and Long (2014) note that caution should be used for their source-side splits in the Alaskan portion of the AASZ because some events may have long paths through the slab. Additionally, we calculated an average fast direction for source-side splits from both studies since we are modeling results over a broader region. This may lead to discrepancies between our models and the source-side splits.

We compare our robust modeling solutions for upper-layer fast directions to local-S splits from Lynner et al. (2024). Here we see the inverse of source-side splits. Iliamna (**Fig. 7b)**, the Eastern Aleutians (**Fig. 7j**), and Okmok (**Fig. 7h**) have some upper-layer models that match local-S splitting. Iliamna and the Eastern Aleutians show good agreement between the peak in the histogram and local-S splitting (around 48° and 35° respectively). Augustine and Katmai show disagreement between robust modeled upper-layer fast directions and local-S splitting. As with source-side splits, we averaged the local-S splits: this could skew the fast directions if there are several local splits with large differences from others.

In addition to some agreement with subslab and local-S splitting, the lower and upper layers of our robust models agree with anisotropic tomography studies of the region. Subslab anisotropy in the AASZ has widely been reported as trench parallel (e.g., Liu et al., 2022; You and Zhao, 2012), though there are reports of trench-perpendicular orientations (Gou et al., 2019). Mantle wedge anisotropy is more varied, with You and Zhao (2012) finding trench-parallel anisotropy and Gou et al. (2019) finding trench-perpendicular anisotropy. A study using Pn phases (which sample the uppermost mantle) also found that fast directions were broadly trench parallel (He and Lü, 2021). These studies have different sensitivities than teleseismic shear wave splitting, so it is encouraging that they reinforce our robust models.

The bulk of the evidence, including previous splitting of different phases, anisotropic tomography, and our robust multilayer models suggests that fast directions in both the subslab and the mantle wedge are either parallel or oblique to the strike of the slab, and therefore subparallel to the trench orientation (**Fig. 7**). Subslab fast directions for Katmai, the Eastern Aleutians are both roughly parallel to the slab strike. For Iliamna and Augustine, they are oblique to slab strike. In the mantle wedge, fast directions for Augustine, and Katmai are parallel to slab strike, and are oblique for Iliamna and the Eastern Aleutians. Only in the case of mantle wedge fast directions for Okmok do we see anything close to orientations perpendicular to slab strike. This suggests that mantle flow in the AASZ is along the strike of the slab, possibly related to the toroidal flow induced by the edge of the slab to the northeast (e.g., Jadamec and Billen, 2012). A tectonic interpretation of our results is shown in **Fig. 8**.

4.3 Best Practices for Layered Anisotropy Modeling

An interesting result of our modeling efforts is that there is oftentimes a mismatch between the single "best-fitting" modeled fast direction, and the largest cluster of fast directions in the robust multilayer models (**Fig. 7** and **Supplemental Figs. S7-10**). Previous studies have shown that modeling multiple layers of anisotropy yields highly nonunique solutions (Latifi et al., 2018; Rümpker et al., 2022). Only examining the "best-fitting" model may therefore be misleading. Importantly, we are only showing those models that are statistically better than a single-layer solution and statistically indistinguishable from the model with the lowest misfit (i.e., the "best-fitting" model). Many other studies that examine multilayered anisotropy from shear wave splitting rely on the best-fitting model, which may bias their interpretation.

One way to reconcile the difference between the lowest-misfit model and all the robust multilayer models is to examine the bandfit misfit as well. As noted in **Section 2.2**, this method compares the calculated model to the error bounds of individual measurements and takes a value of 0 when the model is within bounds and a value of 1 otherwise. Bandfit is shown in **Figs. 5-7**, and all models with a bandfit less than or equal to the lowest bandfit plus four are shown. The bandfit distribution generally agrees with the misfit distribution, and both tend to have peaks at the same fast direction values (**Fig. 7**). In cases where there is a slightly wider distribution in fast directions, such as the lower layer at Iliamna, the bandfit can help to provide better constraints. Even in cases where there is general agreement among the robust models, the bandfit can help to narrow the range of possibilities.

Our layered anisotropy modeling leads us to suggest a pathway to yield the most robust results. First, adequate backazimuthal coverage is required. Because apparent splitting parameters arising from multilayer anisotropy display 90° periodicity, more than 90° of coverage is recommended. While this may be possible for individual long-running stations, it is generally not possible to achieve this through one station alone. Rather, by grouping several stations in proximity, backazimuthal coverage can be increased. The ideal spacing for these groups is largely dependent on the region being modeled. For instance, in subduction zones there may be clear changes in subduction parameters that suggest a specific grouping.

Second, basic statistical analysis is required. In its simplest form, this would compare the best-fitting model against a single-layer case to ensure that there is an improvement in the fit of the data. There are several methods to achieve this. In this study, we utilize an F-test for nested models (Mendenhall and Sincich, 2016). Others have used an adjusted R-squared value (e.g., Walker et al., 2005). However, as shown in our modeling, comparing the best-fitting model alone against the single-layer case may be misleading. The use of the nested F-test allows for the calculation of the entire suite of models that is statistically better than the best-fitting single-layer model. Third, the calculation of an additional metric to determine how well the data is fit by the models is advantageous. Here we use the bandfit method implemented by Eakin and Long (2013). Comparing the suite of models statistically better than the single-layer case and the suite of models within some value of the lowest bandfit should show which parameters are the ideal solution.

Finally, tectonic constraints should be considered when constructing the model. In our study, we constrain the dipping layer using information from Slab2 (Hayes et al., 2018) and paleomagnetic data (Maus et al., 2009). Rümpker et al., (2022) note that by constraining one layer of a grid-search, the solution for the second layer becomes more unique. By using tectonic information to produce an accurate model, it should be possible to yield robust results. For subduction zones, using an HDH setup is ideal given the presence of the slab. Constraining the dipping layer is the easiest, as there is reliable information on the strike and dip from Slab2 (Hayes et al., 2018) and grid-searching for those additional parameters is computationally expensive.

5. Conclusion

Shear wave splitting in the eastern portion of the Alaska-Aleutians subduction zone from our analysis shows signs indicative of multilayered anisotropy. In this study, we model these multiple layers for six subregions. Five of these subregions have a suite of models that are statistically better than a single-layer case. While we test two and three horizontal layer model setups, we ultimately favor a model with horizontal lower and upper layers and a dipping middle – the subslab, slab, and mantle wedge. We find that the dipping slab layer is best approximated with an orientation parallel to paleospreading, while fast directions for the subslab and mantle are best approximated as parallel or oblique to slab strike. Our study argues for the necessity of considering tectonic constraints in shear wave splitting modeling, and the importance of analyzing the statistical significance of models for a robust result.

Acknowledgements

This work was funded in part by NSF OCE 1949210. Figures were made using the Generic Mapping Toolkit (Wessel et al., 2013). The authors report no conflict of interest. We thank Robert Porritt, David Schlaphorst, and one anonymous reviewer for their constructive feedback. We also thank editors John Hopper and Louise Alexander for their assistance.

Data Availability Statement

All seismic data are freely, publicly available through the Data Management Center of the EarthScope Consortium. We provide DOIs for all networks in the **Supplemental Material.** Individual splitting and null measurements are provided in **Table S2**.

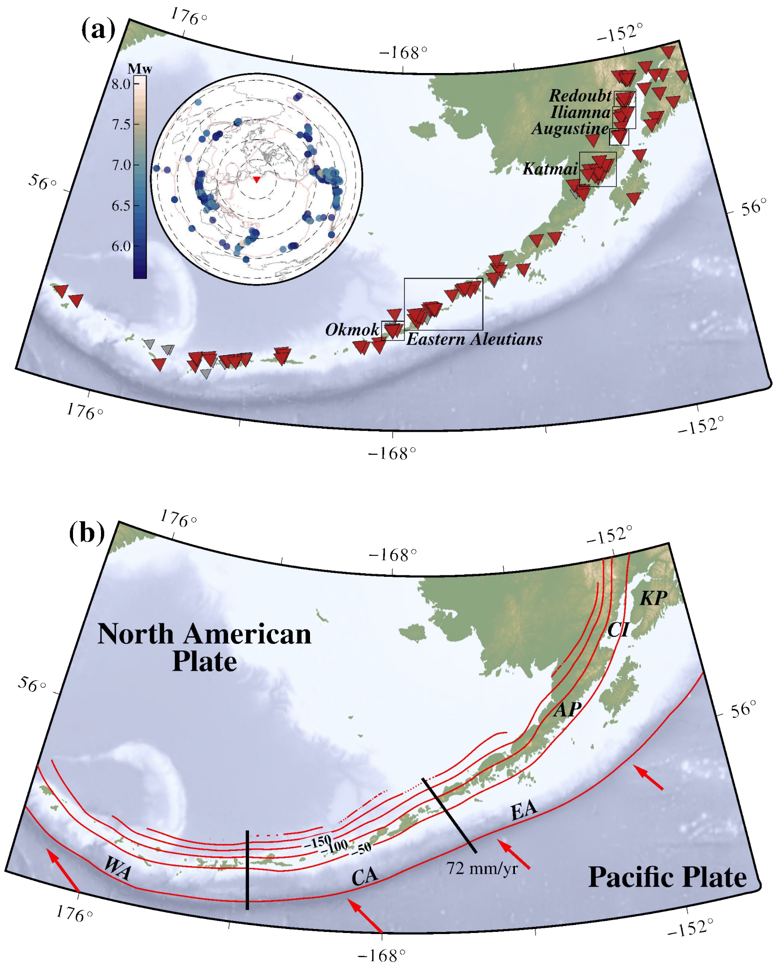

Figure 1: Station and tectonic information. **(a)** All stations used in this study (inverted triangles). Red triangles are those stations with results, while gray triangles were those with no results. Inset displays earthquake locations for calculated splits. Boxes show regions modeled – **Figs. 4 and 7** show these regions in more detail. **(b)** Tectonic map with slab contours (red lines) from Slab2 (Hayes et al., 2018) and motion of the Pacific Plate from a hotspot reference frame (Gripp and Gordon, 2002). Solid black lines delineate the three regions of the Aleutians (Western, Central, and Eastern). AP – Alaskan Peninsula; CA – Central Aleutians; CI – Cook Inlet; EA – Eastern Aleutians; KP – Kenai Peninsula; WA – Western Aleutians.

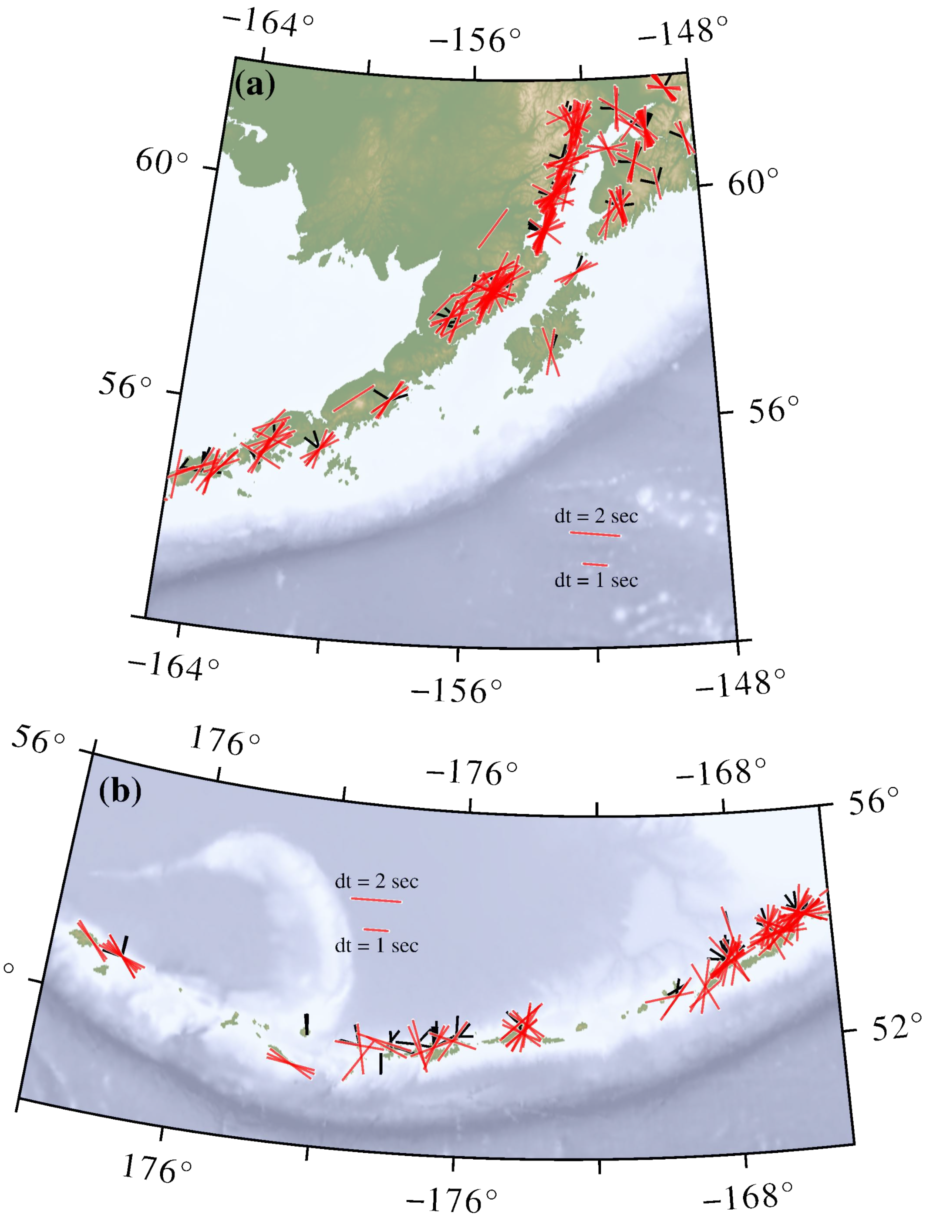

Figure 2: All fair and good splits (in red), plotted at station locations. The orientation of the red bars shows fast direction, while the length shows delay time. Nulls are shown in black with the orientation showing fast direction; length is set to be the same for all nulls. **(a)** Splits for the Eastern Aleutians and Alaskan portion of the AASZ. (**b**) Splits for the Western and Central Aleutians.

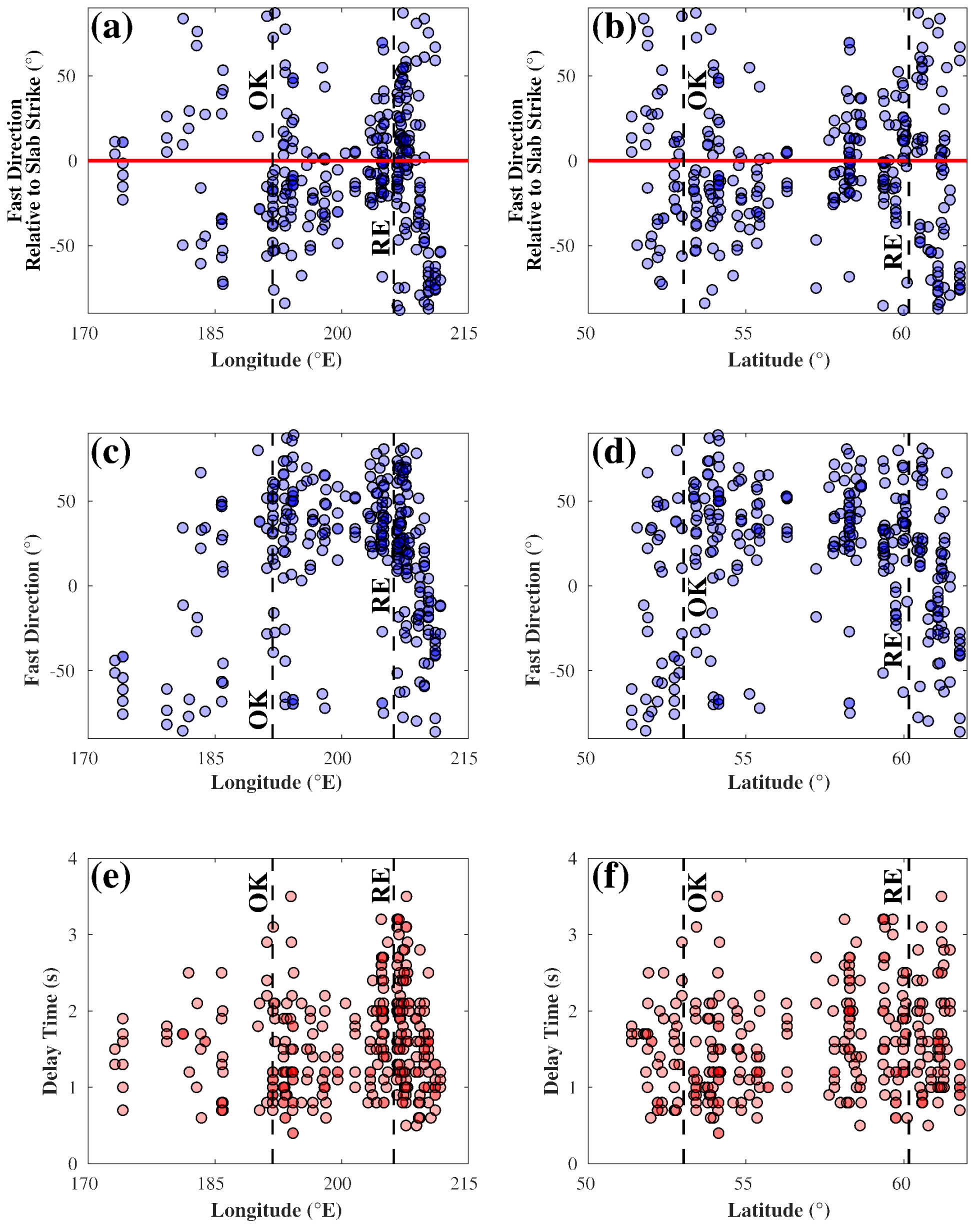

Figure 3: Geographic distribution of fair and good splits. For all six plots, we have marked the location of Mount Okmok (OK) and Mount Redoubt (RE) with a dashed line to help orient readers. (**a-b**) Fast direction relative to the orientation of the trench from Slab2 (Hayes et al., 2018) plotted against longitude and latitude. A value of 0° indicates trench parallel. (**c-d**) Fast direction plotted against longitude and latitude. (**e-f**) Delay time plotted against longitude and latitude.

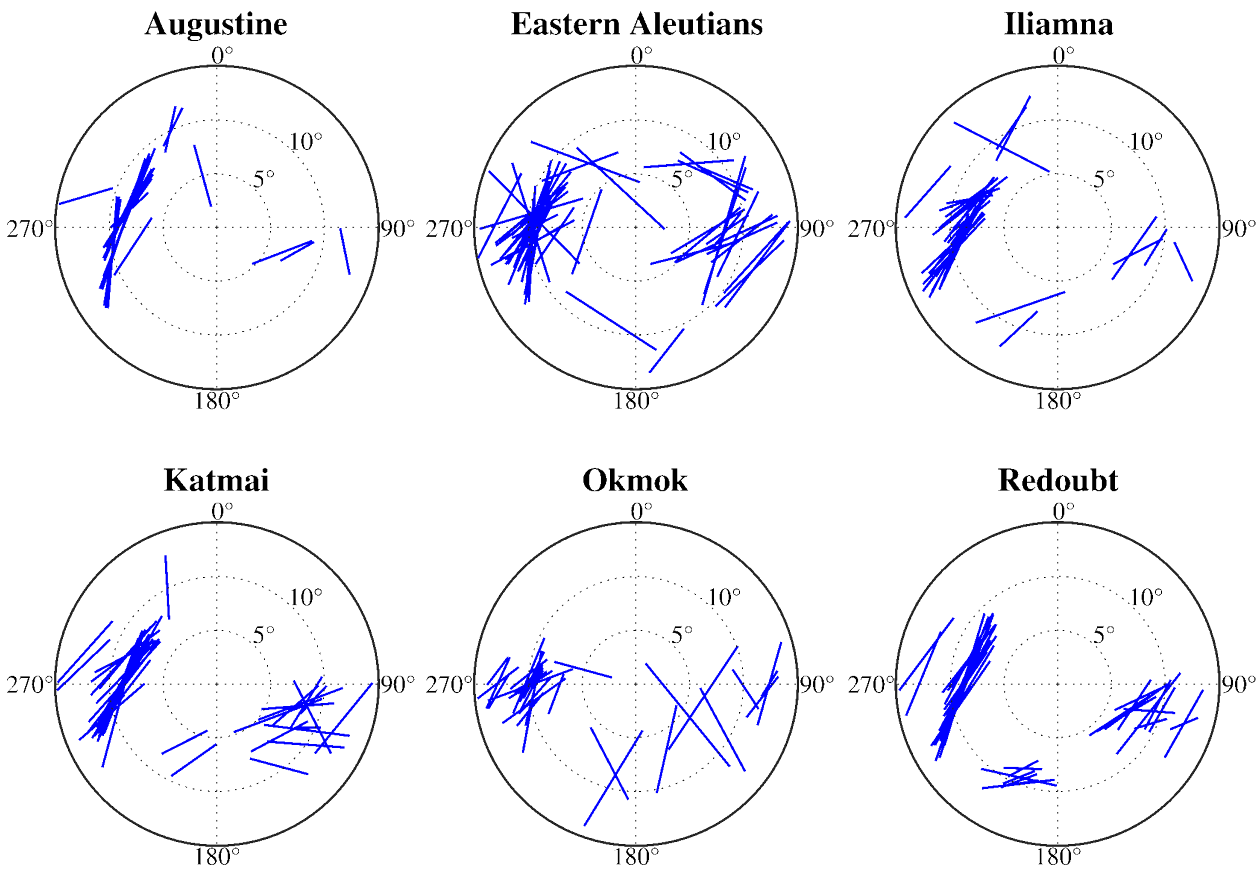

Figure 4: Stereoplots of all splits used in modeling from the regions outlined in **Fig. 1**. Backazimuth of each split is shown along the circumference of the plot (0° to 360°) while inclination angle of each split is shown along the radius (0° to 15°).

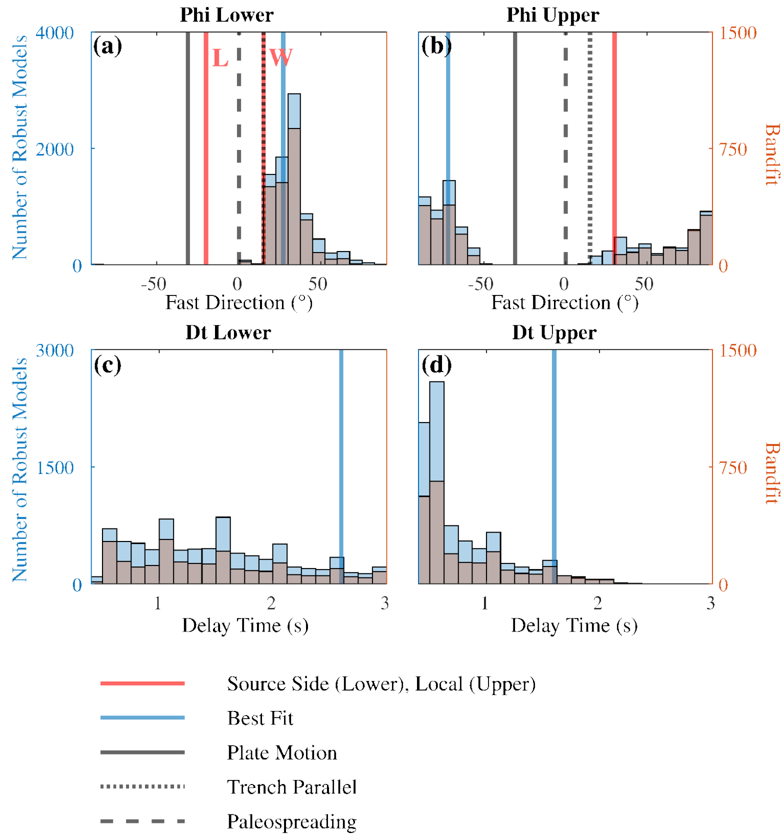

Figure 5: Suite of models at Okmok that are statistically indistinguishable from the model with the lowest misfit, and statistically better than a single-layer case (e.g., robust multilayer models blue bars) for our preferred configuration of three layers with a dipping middle layer oriented parallel to paleospreading. Bandfit shows the set of models within four of the lowest bandfit model (orange bars). **(a-b)** Lower layer and upper layer fast direction suites (Phi Lower and Phi Upper, respectively). Source-side splits are from Lynner and Long (2014) and Walpole et al., (2017). These are marked with an "L" and "W", respectively. Local-S splits are from Lynner et al., (2024), plate motion is from Gripp and Gordon (2002), slab strike orientation is from Slab2 (Hayes et al., 2018), and paleospreading direction is estimated from paleomagnetic data in Maus et al. (2009). **(c-d)** Lower layer and upper layer delay time suites (Dt Lower and Dt Upper, respectively).

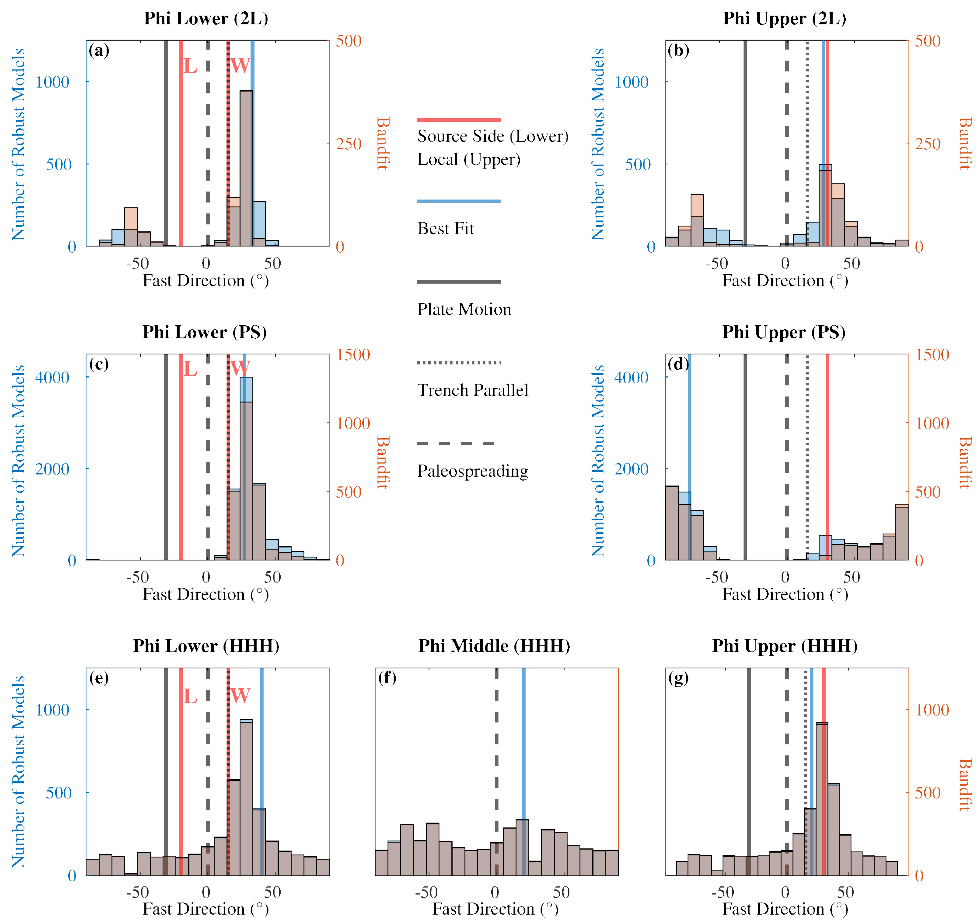

Figure 6: Comparison of fast direction (phi) model suites for **(a-b)** the two-layer (2L), **(c-d)** HDH with middle layer parallel to paleospreading (PS), and **(e-g)** three-layer cases (HHH) at Okmok. Robust multilayer models are shown in blue. Bandfit shows the set of models within four of the lowest bandfit model (shown in orange). Source-side splits are from Lynner and Long (2014) and Walpole et al., (2017). These are marked with an "L" and "W", respectively. Local-S splits are from Lynner et al., (2024), plate motion is from Gripp and Gordon (2002), slab strike orientation is from Slab2 (Hayes et al., 2018), and paleospreading direction is estimated from paleomagnetic data in Maus et al. (2009).

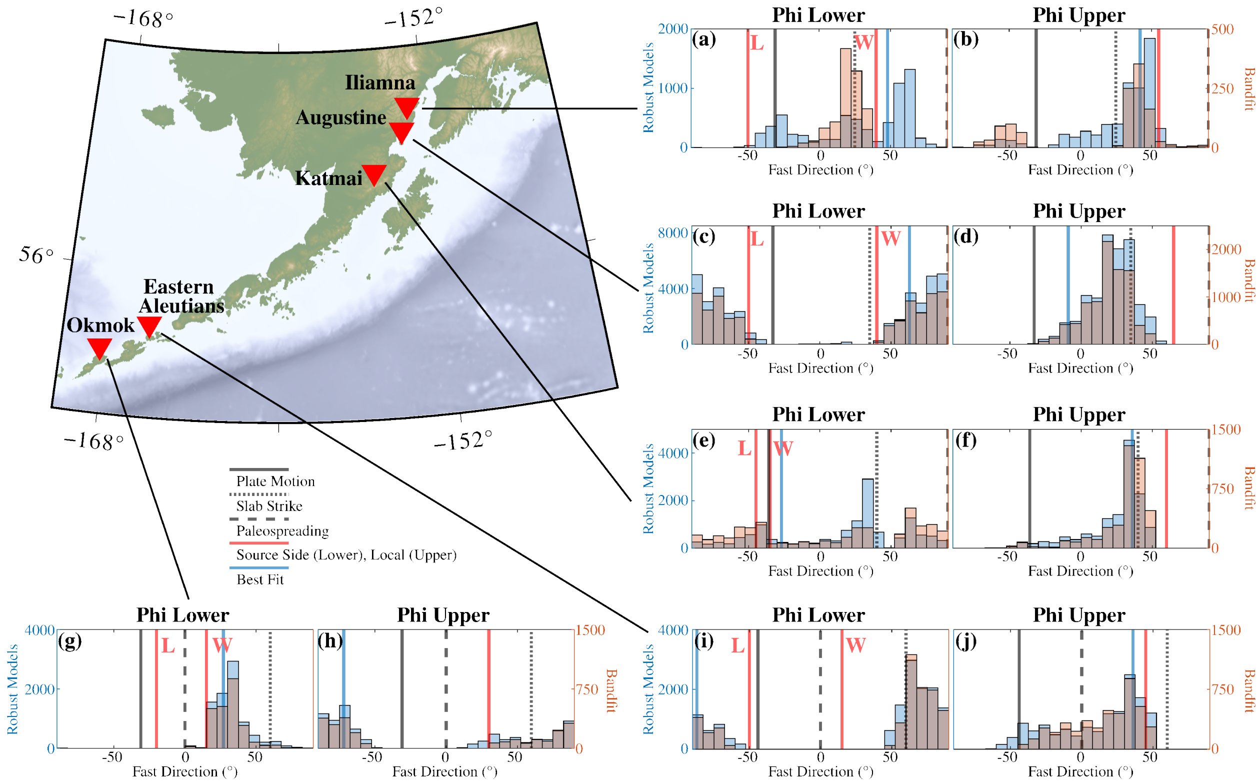

Figure 7: Preferred configuration (HDH with middle dipping layer oriented parallel to paleospreading) robust models for all regions, shown in blue. Only fast directions (phi) are shown (see main text for further details). Bandfit shows the set of models within four of the lowest bandfit model (shown in orange). Source-side splits are from Lynner and Long (2014) and Walpole et al., (2017). These are marked with an "L" and "W", respectively. Local-S splits are from Lynner et al., (2024), plate motion is from Gripp and Gordon (2002), slab strike orientation is from Slab2 (Hayes et al., 2018), and paleospreading direction is estimated from paleomagnetic data in Maus et al. (2009).

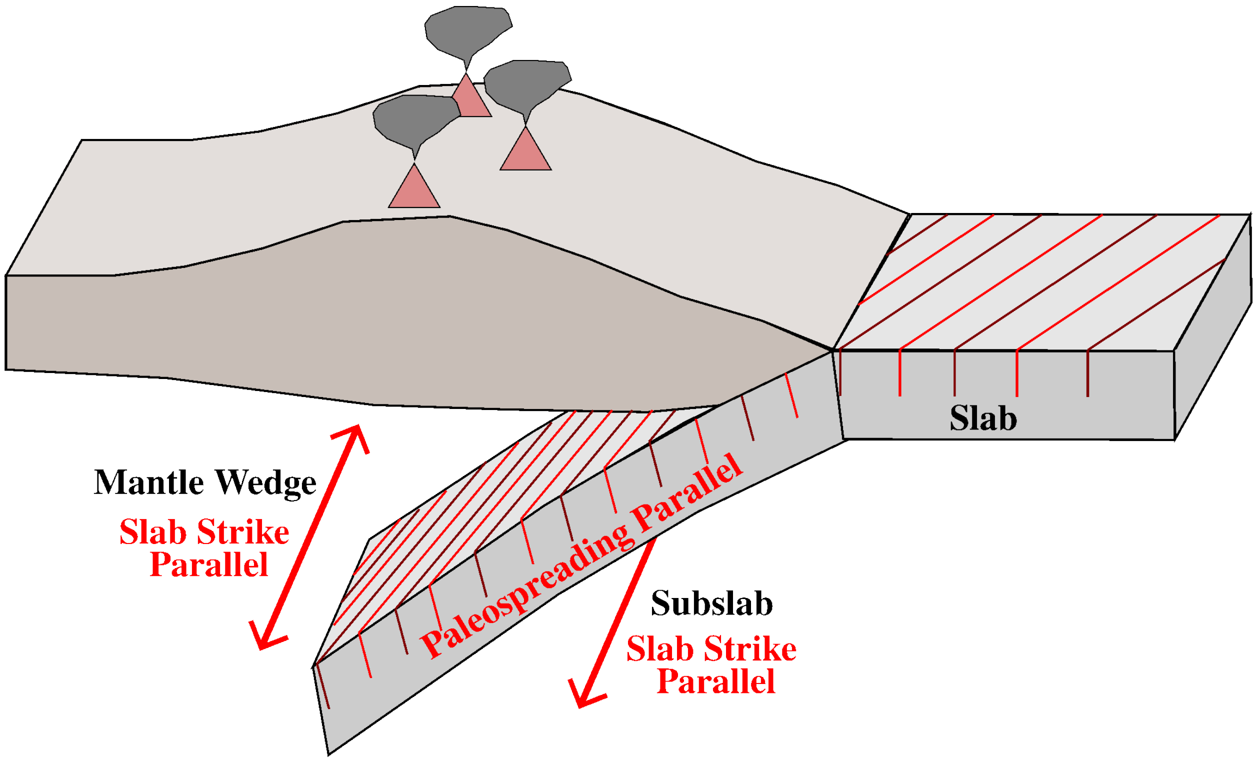

Figure 8: A cartoon schematic of our preferred interpretation of anisotropy beneath Augustine, the Eastern Aleutians, Iliamna, Katmai, and Okmok. Anisotropy is shown in red. For the mantle wedge and the subslab, our preferred model is anisotropy oriented parallel to slab strike. In the slab itself, our modeling and previous studies suggests anisotropy oriented parallel to paleospreading.

Table 1: Peak of fast direction histogram for suite of models that are statistically indistinguishable from the lowest misfit model, and statistically better than the single-layer case. Histograms for the paleospreading case can be seen in **Figure 7**, and all others can be seen in the **Supplementary Material**. Phi Lower – fast direction in the lowest layer of the model; Phi Upper – fast direction in the topmost layer of the model; 2L – two layer case; PS – paleospreading case; HHH – three layer case.

	2L		**PS**		**HHH**	
	Phi Lower	*Phi Upper*	*Phi Lower*	*Phi Upper*	*Phi Lower*	*Phi Upper*
Augustine	83	30	84	33	71	23
EAL	57	30	63	33	62	33
Iliamna	57	36	63	48	52	42
Katmai	30	30	33	33	23	33
Okmok	23	30	33	-72	23	30

References

Abgarmi, B., & Arda Özacar, A. (2017). M-Split: A Graphical User Interface to Analyze Multilayered Anisotropy from Shear-Wave Splitting. Seismological Research Letters, 88(4), 1146-1155. https://doi.org/10.1785/0220170020

Arcay, D., Doin, M. P., Tric, E., Bousquet, R., & De Capitani, C. (2006). Overriding plate thinning in subduction zones: Localized convection induced by slab dehydration. Geochemistry, Geophysics, Geosystems, 7(2). https://doi.org/10.1029/2005gc001061

Audet, P. (2013). Seismic anisotropy of subducting oceanic uppermost mantle from fossil spreading. Geophysical research letters, 40(1), 173-177. https://doi.org/10.1029/2012gl054328

Bowman, J. R., & Ando, M. (1987). Shear-wave splitting in the upper-mantle wedge above the Tonga subduction zone. Geophysical Journal International, 88(1), 25-41. https://doi.org/10.1111/j.1365-246x.1987.tb01367.x

Brechner, S., Klinge, K., Krüger, F., & Plenefisch, T. (1998). Backazimuthal variations of splitting parameters of teleseismic SKS phases observed at the broadband stations in Germany. In Geodynamics of Lithosphere & Earth's Mantle: Seismic Anisotropy as a Record of the Past and Present Dynamic Processes (pp. 305-331). Birkhäuser Basel. https://doi.org/10.1007/978-3-0348-8777-9_5

Chen, K. H., Tseng, Y. L., Furumura, T., & Kennett, B. L. (2015). Anisotropy in the subducting slab: Observations from Philippine Sea plate events in Taiwan. Geophysical Research Letters, 42(23), 10-248. https://doi.org/10.1002/2015gl066227

Chevrot, S. (2000). Multichannel analysis of shear wave splitting. Journal of Geophysical Research: Solid Earth, 105(B9), 21579-21590. https://doi.org/10.1029/2000jb900199

Chevrot, S., & Van Der Hilst, R. D. (2003). On the effects of a dipping axis of symmetry on shear wave splitting measurements in a transversely isotropic medium. Geophysical Journal International, 152(2), 497-505. https://doi.org/10.1046/j.1365-246x.2003.01865.x

Christensen, D. H., & Abers, G. A. (2010). Seismic anisotropy under central Alaska from SKS splitting observations. Journal of Geophysical Research: Solid Earth, 115(B4). https://doi.org/10.1029/2009jb006712

Currie, C. A., Cassidy, J. F., Hyndman, R. D., & Bostock, M. G. (2004). Shear wave anisotropy beneath the Cascadia subduction zone and western North American craton. Geophysical Journal International, 157(1), 341-353. https://doi.org/10.1111/j.1365-246x.2004.02175.x

Currie, C. A., Huismans, R. S., & Beaumont, C. (2008). Thinning of continental backarc lithosphere by flow-induced gravitational instability. Earth and Planetary Science Letters, 269(3-4), 436-447. https://doi.org/10.1016/j.epsl.2008.02.037

Deng, J., Long, M. D., Creasy, N., Wagner, L., Beck, S., Zandt, G., ... & Minaya, E. (2017). Lowermost mantle anisotropy near the eastern edge of the Pacific LLSVP: constraints from SKS–SKKS splitting intensity measurements. Geophysical Journal International, 210(2), 774-786. https://doi.org/10.1093/gji/ggx190

Eakin, C. M., & Long, M. D. (2013). Complex anisotropy beneath the Peruvian flat slab from frequency-dependent, multiple-phase shear wave splitting analysis. Journal of Geophysical Research: Solid Earth, 118(9), 4794-4813. https://doi.org/10.1002/jgrb.50349

Faccenda, M., Burlini, L., Gerya, T. V., & Mainprice, D. (2008). Fault-induced seismic anisotropy by hydration in subducting oceanic plates. Nature, 455(7216), 1097-1100. https://doi.org/10.1038/nature07376

Faccenda, M., & Capitanio, F. A. (2012). Development of mantle seismic anisotropy during subduction-induced 3-D flow. Geophysical Research Letters, 39(11). https://doi.org/10.1029/2012gl051988

Faccenda, M., & Capitanio, F. A. (2013). Seismic anisotropy around subduction zones: Insights from three-dimensional modeling of upper mantle deformation and SKS splitting calculations. Geochemistry, Geophysics, Geosystems, 14(1), 243-262. https://doi.org/10.1002/ggge.20055

Feng, L., Liu, C., & Ritzwoller, M. H. (2020). Azimuthal anisotropy of the crust and uppermost mantle beneath Alaska. Journal of Geophysical Research: Solid Earth, 125(12), e2020JB020076. https://doi.org/10.1029/2020jb020076

Fouch, M. J., & Rondenay, S. (2006). Seismic anisotropy beneath stable continental interiors. Physics of the Earth and Planetary Interiors, 158(2-4), 292-320. https://doi.org/10.1016/j.pepi.2006.03.024

Gao, S. S., Liu, K. H., & Abdelsalam, M. G. (2010). Seismic anisotropy beneath the Afar Depression and adjacent areas: Implications for mantle flow. Journal of Geophysical Research: Solid Earth, 115(B12). https://doi.org/10.1029/2009jb007141

Gou, T., Zhao, D., Huang, Z., & Wang, L. (2019). Aseismic deep slab and mantle flow beneath Alaska: Insight from anisotropic tomography. Journal of Geophysical Research: Solid Earth, 124(2), 1700-1724. https://doi.org/10.1029/2018jb016639

Gripp, A. E., & Gordon, R. G. (2002). Young tracks of hotspots and current plate velocities. Geophysical Journal International, 150(2), 321-361. https://doi.org/10.1046/j.1365-246x.2002.01627.x

Hall, C. E., Fischer, K. M., Parmentier, E. M., & Blackman, D. K. (2000). The influence of plate motions on three-dimensional back arc mantle flow and shear wave splitting. Journal of Geophysical Research: Solid Earth, 105(B12), 28009-28033. https://doi.org/10.1029/2000jb900297

Hammond, J. O., Kendall, J. M., Wookey, J., Stuart, G. W., Keir, D., & Ayele, A. (2014). Differentiating flow, melt, or fossil seismic anisotropy beneath Ethiopia. Geochemistry, Geophysics, Geosystems, 15(5), 1878-1894. https://doi.org/10.1002/2013gc005185

Hanna, J., & Long, M. D. (2012). SKS splitting beneath Alaska: Regional variability and implications for subduction processes at a slab edge. Tectonophysics, 530, 272-285. https://doi.org/10.1016/j.tecto.2012.01.003

Hayes, G. P., Moore, G. L., Portner, D. E., Hearne, M., Flamme, H., Furtney, M., & Smoczyk, G. M. (2018). Slab2, a comprehensive subduction zone geometry model. Science, 362(6410), 58-61. https://doi.org/10.1126/science.aat4723

Healy, D., Reddy, S. M., Timms, N. E., Gray, E. M., & Brovarone, A. V. (2009). Trench-parallel fast axes of seismic anisotropy due to fluid-filled cracks in subducting slabs. Earth and Planetary Science Letters, 283(1-4), 75-86. https://doi.org/10.1016/j.epsl.2009.03.037

Jadamec, M. A., & Billen, M. I. (2010). Reconciling surface plate motions with rapid three-dimensional mantle flow around a slab edge. Nature, 465(7296), 338-341. https://doi.org/10.1038/nature09053

Jadamec, M. A., & Billen, M. I. (2012). The role of rheology and slab shape on rapid mantle flow: Three-dimensional numerical models of the Alaska slab edge. Journal of Geophysical Research: Solid Earth, 117(B2). https://doi.org/10.1029/2011jb008563

Jung, H. (2017). Crystal preferred orientations of olivine, orthopyroxene, serpentine, chlorite, and amphibole, and implications for seismic anisotropy in subduction zones: a review. Geosciences Journal, 21, 985-1011. https://doi.org/10.1007/s12303-017-0045-1

Jung, H., & Karato, S. I. (2001). Water-induced fabric transitions in olivine. Science, 293(5534), 1460-1463. https://doi.org/10.1126/science.1062235

Jung, H., Katayama, I., Jiang, Z., Hiraga, T., & Karato, S. I. (2006). Effect of water and stress on the lattice-preferred orientation of olivine. Tectonophysics, 421(1-2), 1-22. https://doi.org/10.1016/j.tecto.2006.02.011

Karato, S. I., Jung, H., Katayama, I., & Skemer, P. (2008). Geodynamic significance of seismic anisotropy of the upper mantle: New insights from laboratory studies. *Annu. Rev. Earth Planet. Sci.*, *36*, 59-95. https://doi.org/10.1146/annurev.earth.36.031207.124120

Karlowska, E., Bastow, I. D., Rondenay, S., Martin-Short, R., & Allen, R. M. (2021). The development of seismic anisotropy below south-central Alaska: evidence from local earthquake shear wave splitting. *Geophysical Journal International*, *225*(1), 548-554. https://doi.org/10.1093/gji/ggaa603

Lallemand, S., Heuret, A., & Boutelier, D. (2005). On the relationships between slab dip, back-arc stress, upper plate absolute motion, and crustal nature in subduction zones. Geochemistry, Geophysics, Geosystems, 6(9). https://doi.org/10.1029/2005gc000917

Latifi, K., Kaviani, A., Rümpker, G., Mahmoodabadi, M., Ghassemi, M. R., & Sadidkhouy, A. (2018). The effect of crustal anisotropy on SKS splitting analysis—synthetic models and real-data observations. Geophysical Journal International, 213(2), 1426-1447. https://doi.org/10.1093/gji/ggy053

Lee, J., Jung, H., Klemd, R., Tarling, M. S., & Konopelko, D. (2020). Lattice preferred orientation of talc and implications for seismic anisotropy in subduction zones. Earth and Planetary Science Letters, 537, 116178. https://doi.org/10.1016/j.epsl.2020.116178

Lee, J., Mookherjee, M., Kim, T., Jung, H., & Klemd, R. (2021). Seismic anisotropy in subduction zones: Evaluating the role of Chloritoid. Frontiers in Earth Science, 9, 644958. https://doi.org/10.3389/feart.2021.644958

Levin, V., Menke, W., & Park, J. (1999). Shear wave splitting in the Appalachians and the Urals: a case for multilayered anisotropy. Journal of Geophysical Research: Solid Earth, 104(B8), 17975-17993. https://doi.org/10.1029/1999jb900168

Liu, C., Zhang, S., Sheehan, A. F., & Ritzwoller, M. H. (2022). Surface Wave Isotropic and Azimuthally Anisotropic Dispersion Across Alaska and the Alaska-Aleutian Subduction Zone. Journal of Geophysical Research: Solid Earth, 127(11), e2022JB024885. https://doi.org/10.1029/2022jb024885

Long, M. D., Hager, B. H., De Hoop, M. V., & Van Der Hilst, R. D. (2007). Two-dimensional modelling of subduction zone anisotropy with application to southwestern Japan. Geophysical Journal International, 170(2), 839-856. https://doi.org/10.1111/j.1365-246x.2007.03464.x

Long, M. D., & Silver, P. G. (2008). The subduction zone flow field from seismic anisotropy: A global view. Science, 319(5861), 315-318. https://doi.org/10.1126/science.1150809

Long, M. D., & Silver, P. G. (2009). Mantle flow in subduction systems: The subslab flow field and implications for mantle dynamics. Journal of Geophysical Research: Solid Earth, 114(B10). https://doi.org/10.1029/2008jb006200

Long, M. D., & Wirth, E. A. (2013). Mantle flow in subduction systems: The mantle wedge flow field and implications for wedge processes. Journal of Geophysical Research: Solid Earth, 118(2), 583-606. https://doi.org/10.1002/jgrb.50063

Lynner, C. (2021). Anisotropy-revealed change in hydration along the Alaska subduction zone. Geology, 49(9), 1122-1125. https://doi.org/10.1130/geol.s.14582757.v1

Lynner, C., & Long, M. D. (2014). Sub-slab anisotropy beneath the Sumatra and circum-Pacific subduction zones from source-side shear wave splitting observations. Geochemistry, Geophysics, Geosystems, 15(6), 2262-2281. https://doi.org/10.1002/2014gc005239

Lynner, C., Toro-Acosta, C., Paulson, E., & Birkey, A. (2024). Local-S shear wave splitting along the length of the Alaska-aleutian subduction zone. Geophysical Journal International. https://doi.org/10.1093/gji/ggae107

Maus, S., Barckhausen, U., Berkenbosch, H., Bournas, N., Brozena, J., Childers, V., ... & Caratori Tontini, F. (2009). EMAG2: A 2–arc min resolution Earth Magnetic Anomaly Grid compiled from satellite, airborne, and marine magnetic measurements. Geochemistry, Geophysics, Geosystems, 10(8). https://doi.org/10.1029/2009gc002471

McKenzie, D. P. (1969). Speculations on the consequences and causes of plate motions. Geophysical Journal International, 18(1), 1-32. https://doi.org/10.1111/j.1365-246x.1969.tb00259.x

McPherson, A. M., Christensen, D. H., Abers, G. A., & Tape, C. (2020). Shear wave splitting and mantle flow beneath Alaska. Journal of Geophysical Research: Solid Earth, 125(4), e2019JB018329. https://doi.org/10.1029/2019jb018329

Mendenhall, W. M., & Sincich, T. L. (2016). Statistics for Engineering and the Sciences. CRC Press.

Nathan, E. M., Hariharan, A., Florez, D., & Fischer, K. M. (2021). Multi-Layer Seismic Anisotropy Beneath Greenland. Geochemistry, Geophysics, Geosystems, 22(5), e2020GC009512. https://doi.org/10.1002/essoar.10505663.1

Özalaybey, S., & Savage, M. K. (1994). Double-layer anisotropy resolved from S phases. Geophysical Journal International, 117(3), 653-664. https://doi.org/10.1111/j.1365-246x.1994.tb02460.x

Paczkowski, K., Montési, L. G., Long, M. D., & Thissen, C. J. (2014). Three-dimensional flow in the subslab mantle. Geochemistry, Geophysics, Geosystems, 15(10), 3989-4008. https://doi.org/10.1002/2014gc005441

Perttu, A., Christensen, D., Abers, G., & Song, X. (2014). Insights into mantle structure and flow beneath Alaska based on a decade of observations of shear wave splitting. Journal of Geophysical Research: Solid Earth, 119(11), 8366-8377. https://doi.org/10.1002/2014jb011359

Reiss, M. C., Rümpker, G., & Wölbern, I. (2018). Large-scale trench-normal mantle flow beneath central South America. Earth and Planetary Science Letters, 482, 115-125. https://doi.org/10.1016/j.epsl.2017.11.002

Richards, C., Tape, C., Abers, G. A., & Ross, Z. E. (2021). Anisotropy variations in the Alaska subduction zone based on shear-wave splitting from intraslab earthquakes. Geochemistry, Geophysics, Geosystems, 22(5), e2020GC009558. https://doi.org/10.1029/2020gc009558

Rümpker, G., Kaviani, A., Link, F., Reiss, M. C., & Komeazi, A. (2022). Testing Observables for Teleseismic Shear-Wave Splitting Inversions: Ambiguities of Intensities, Parameters, and Waveforms. In AGU Fall Meeting Abstracts (Vol. 2022, pp. DI12A-05). https://doi.org/10.4401/ag-8870

Savage, M. K. (1999). Seismic anisotropy and mantle deformation: what have we learned from shear wave splitting?. Reviews of Geophysics, 37(1), 65-106. https://doi.org/10.1029/98rg02075

Silver, P. G. (1996). Seismic anisotropy beneath the continents: Probing the depths of geology. Annual review of earth and planetary sciences, 24(1), 385-432. https://doi.org/10.1146/annurev.earth.24.1.385

Silver, P. G., & Chan, W. W. (1991). Shear wave splitting and subcontinental mantle deformation. Journal of Geophysical Research: Solid Earth, 96(B10), 16429-16454. https://doi.org/10.1029/91jb00899

Silver, P. G., & Savage, M. K. (1994). The interpretation of shear-wave splitting parameters in the presence of two anisotropic layers. Geophysical Journal International, 119(3), 949-963. https://doi.org/10.1111/j.1365-246x.1994.tb04027.x

Song, T. R. A., & Kim, Y. (2012). Anisotropic uppermost mantle in young subducted slab underplating Central Mexico. Nature Geoscience, 5(1), 55-59. https://doi.org/10.1038/ngeo1342

Venereau, C. M. A., Martin-Short, R., Bastow, I. D., Allen, R. M., & Kounoudis, R. (2019). The role of variable slab dip in driving mantle flow at the eastern edge of the Alaskan subduction margin: Insights from shear-wave splitting. Geochemistry, Geophysics, Geosystems, 20(5), 2433-2448. https://doi.org/10.1029/2018gc008170

Walker, A. M., & Wookey, J. (2012). MSAT—A new toolkit for the analysis of elastic and seismic anisotropy. Computers & Geosciences, 49, 81-90. https://doi.org/10.1016/j.cageo.2012.05.031

Walker, K. T., Bokelmann, G. H., & Klemperer, S. L. (2001). Shear-wave splitting to test mantle deformation models around Hawaii. Geophysical Research Letters, 28(22), 4319-4322. https://doi.org/10.1029/2001gl013299

Walker, K. T., Bokelmann, G. H. R., Klemperer, S. L., & Bock, G. (2005). Shear-wave splitting around the Eifel hotspot: evidence for a mantle upwelling. Geophysical Journal International, 163(3), 962-980. https://doi.org/10.1111/j.1365-246x.2005.02636.x

Walpole, J., Wookey, J., Kendall, J. M., & Masters, T. G. (2017). Seismic anisotropy and mantle flow below subducting slabs. Earth and Planetary Science Letters, 465, 155-167.

Wang, Y., & Tape, C. (2014). Seismic velocity structure and anisotropy of the Alaska subduction zone based on surface wave tomography. Journal of Geophysical Research: Solid Earth, 119(12), 8845-8865. https://doi.org/10.1016/j.epsl.2017.02.023

Wessel, P., Smith, W. H., Scharroo, R., Luis, J., & Wobbe, F. (2013). Generic mapping tools: improved version released. Eos, Transactions American Geophysical Union, 94(45), 409-410. https://doi.org/10.1002/2013eo450001

Wirth, E. A., & Long, M. D. (2012). Multiple layers of seismic anisotropy and a low-velocity region in the mantle wedge beneath Japan: Evidence from teleseismic receiver functions. Geochemistry, Geophysics, Geosystems, 13(8). https://doi.org/10.1029/2012gc004180

Wüstefeld, A., Bokelmann, G., Zaroli, C., & Barruol, G. (2008). SplitLab: A shear-wave splitting environment in Matlab. Computers & Geosciences, 34(5), 515-528. https://doi.org/10.1016/j.cageo.2007.08.002

Yang, X., Fischer, K. M., & Abers, G. A. (1995). Seismic anisotropy beneath the Shumagin Islands segment of the Aleutian-Alaska subduction zone. Journal of Geophysical Research: Solid Earth, 100(B9), 18165-18177. https://doi.org/10.1029/95jb01425

Yang, B. B., Gao, S. S., Liu, K. H., Elsheikh, A. A., Lemnifi, A. A., Refayee, H. A., & Yu, Y. (2014). Seismic anisotropy and mantle flow beneath the northern Great Plains of North America. Journal of Geophysical Research: Solid Earth, 119(3), 1971-1985. https://doi.org/10.1002/2013jb010561

Yang, Y., Gao, S. S., Liu, K. H., Kong, F., & Fu, X. (2021). Mantle flow in the vicinity of the eastern edge of the Pacific-Yakutat slab: Constraints from shear wave splitting analyses. Journal of Geophysical Research: Solid Earth, 126(9), e2021JB022354. https://doi.org/10.1029/2021jb022354

You, T., & Zhao, D. (2012). Seismic anisotropy and heterogeneity in the Alaska subduction zone. Geophysical Journal International, 190(1), 629-649. https://doi.org/10.1111/j.1365-246x.2012.05512.x